Chapter 2
GIS-Based Landslide Susceptibility Mapping in Eastern Boundary Zone of Northeast India in Compliance with Indo-Burmese Subduction Tectonics

Arnab Sengupta and Sankar Kumar Nath

Abstract The Eastern Boundary Zone of Northeast India, comprising the Indian States of Manipur, Mizoram and Nagaland, suffers immensely under the impact of frequent devastating landslides that results in widespread damage and casualty. A rough estimate of the decadal intensity of landslides from an inventory spanning over half a century calls for systematic assessment of landslide hazard and risk in the region for its effective mitigation and management. Landslide Susceptibility Zonation is the most fundamental step in that direction wherein spatial distribution of Landslide Susceptibility Index (LSI) is established through integrating nineteen causative factors, viz. surface geology, landform, lineament density, elevation, distance to lineament, slope angle, aspect, drainage density, distance to drainage, terrain ruggedness index, plan and profile curvature, normalized difference vegetation index, landuse/landcover, distance to road, road density, rainfall, earthquake epicentre proximity and peak ground acceleration rationally on GIS platform in 1:50,000 scale by following a multivariate statistics-based Logistic Regression (LR) procedure. This classifies the terrain into None, Low, Moderate, High, Very High and Severe susceptible zones on a raster map display, which is inevitably validated through statistical accuracy test by drawing a comparison with the 30% landslide inventory test dataset which exhibited 73% accuracy level. This landslide susceptibility map will invariably help the urban planners and the decision-makers in effective landslide risk mitigation and spatial design.

Keywords Landslide Susceptibility Zones · Indo-Barmic Subduction · Northeast India · Eastern Boundary Zone

A. Sengupta · S. K. Nath (✉)
Department of Geology and Geophysics, Indian Institute of Technology Kharagpur, Kharagpur, West Bengal, India
e-mail: nath@gg.iitkgp.ac.in

P. K. Shit et al. (eds.), *Geospatial Technology for Environmental Hazards*, Advances in Geographic Information Science, https://doi.org/10.1007/978-3-030-75197-5_2

2.1 Introduction

Landslide is a process associated with the downward movements of soil, rock, debris, artificial fill and/or a mixture of all of these. Landslide occurs due to both physical and man-made activities. Physical activities consist of an impending earthquake, volcanic eruptions, tectonic activities, torrential rainfall, storm, etc., while man-made activities include unscientific construction, unmannered tourism and so on. Rainfall-induced landslides are very common around the globe. Current estimates of landslide impacts suggest that they cause thousands of fatalities annually (Froude and Petley (2018); Petley (2012) and economic loss worth billions of US dollars (Dilley et al., 2005; CRED, n.d.) as shown in Fig. 2.1(a). Global warming, climate change and rising temperature are expected to trigger landslides, especially in mountainous regions with snow and ice and cover. In India, a total of 0.42 million km^2 or 12.6% of the landmass is imperil due to landslides of which an

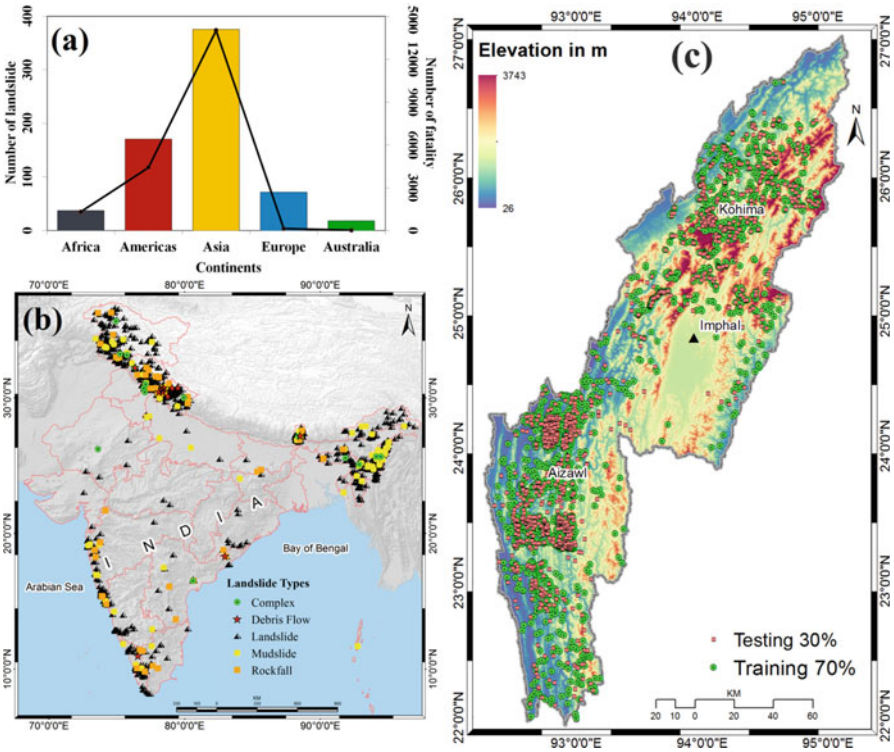

Fig. 2.1 Location map of the study region. (**a**) Continent-wise landslide inventory data (bar graph) and line graph are showing the number of fatalities (source: CRED, n.d.). (**b**) Landslide inventory map of the Indian subcontinent. (**c**) Landslide inventory (training and testing) data in the Eastern Boundary Zone of Northeast India comprising of the Indian States of Manipur, Mizoram and Nagaland

approximate 0.18 million km^2 falls is in the Northeast Himalayan province of India; an approximate 0.14 million km^2 lays in the Northwest Himalaya; 0.09 million km^2 is in the Western Ghats and Konkan hills; and an approximate 0.01 million km^2 is in the Eastern Ghats causing an estimated damage cost of around 2–5 billion US dollars and 25% of annual deaths as depicted in Fig. 2.1(b).

The Eastern Boundary Zone in Northeast India comprising the Indian States of Manipur, Mizoram and Nagaland is a landslide-prone region as depicted in Fig. 2.1 (c). The study region covers around 60,025.56 km^2 comprising of 12 small towns. It is surrounded by the Tertiary hills of Mizoram, Manipur and Nagaland with a maximum altitude of 3743 m with steep to moderate slopes. Geologically, the region is classified into pre-Cambrian to Quaternary era. Tertiary rocks of the Disang and Baraingroup that consists of shale and sandstone are most predominant in the territory, which on weathering becomes platy and splintery, proving the most ideal state for landsliding. The terrain is also seismogenic being one of the most active regions of the world and according to BIS (2002); it falls under Seismic Zone V with frequent moderate to large magnitude earthquakes visiting the terrain causing extensive damage to both life and property.

Landslide susceptibility mapping in the Eastern Boundary Block of Northeast India, using various algorithms, has already been attempted by several researchers, viz. Laldintluanga et al. (2016); Pathak (2016); Balamurugan et al. (2016); Lallianthanga and Lalbiakmawia (2013a, 2013b, 2014); Lallianthanga et al. (2013); Barman and Srinivasa Rao (2019); Lallianthanga and Laltanpuia (2014); Balamurugan and Ramesh (2016); Pachuau (2019); Khatsu and Van Westen (2005); Roy et al. (2019); Sema et al. (2017); and Singh et al. (2011). A comprehensive literature review unfolds that earlier works have been performed at the site-specific scale on a slope-slope basis and not in the regional scale. In this study, we, however, considered the entire Eastern Boundary Zone of the Northeast India comprising the Indian States of Manipur, Mizoram and Nagaland as a unit tectonic block for an overall understanding of the probability of landslide occurrence in the terrain using an ensemble of Remote Sensing-GIS for chocking out a pre-disaster landslide risk mitigation strategy to be put in place and to perform precursory damage estimation for insurance coverage purposes.

2.2 Data and Methodology

Spatial and Non-spatial Data

In order to achieve the GIS-based landslide susceptibility zonation, there is a requirement of spatial and non-spatial data as illustrated in Table 2.1.

Table 2.1 Spatial and non-spatial data used in the present study

Data	Causative layers	Source
Geology map	Surface geology map	Geological Survey of India
Lineament map	Lineament density and distance to lineament	Dasgupta et al. (2000), National Mission on Geomorphological and Lineament Mapping, http://bhuvan.nrsc.gov.in/gis/thematic/index.php
Road Network	Road density and distance to road	Open Street Map and Google Earth
Earthquake catalogue	Epicentre proximity	Nath et al. (2017), USGS, IMD and ISC
Rainfall data	Rainfall map	India Meteorological Department and Tropical Rainfall Measuring Mission
ALOS PALSAR DEM (30 m)	Slope angle, slope aspect, landform, elevation, Drainage density, distance to drainage, plan curvature, Terrain ruggedness index	Japan Aerospace Exploration Agency
Landsat 8 (30 m)	Normalized difference vegetation index	United States Geological Survey
GlobCover land cover map	Land use/land cover	European Space Agency
Seismic shaking	Surface consistent peak ground acceleration	Nath and Thingbaijam (2012)

Multivariate Statistics: Logistic Regression (LR)

Among a wide range of statistical methods proposed for the assessment of landslide susceptibility distribution, Logistic Regression (LR) has proven to provide one of the most reliable classification technique (Reichenbach et al., 2018; Guzzetti et al., 2006; Mancini et al., 2010; Hadmoko et al., 2017; Bai et al., 2011; Mathew et al., 2009; Lee & Pradhan, 2007; Nandi & Shakoor, 2010). LR simulates the probability of a certain class or event. It uses a logistic function to model a binary dependent variable even though many complex extensions exist. The aim of LR model is to establish a relation between the existing and the absent landslides. The advantage of this method is that the dependent variable can have only two values, i.e. occurring or non-occurring, and those predicted values can be interpreted as the probability since they are inhibited to lay in the interval between 0 and 1 Dai and Lee (2002). In the Logistic Regression analysis, there are some dependent variables that correlate with an independent variable. The predicted value ranges from 0 to 1, and it can be defined as the landslide susceptibility index. The road map of the algorithm worked out in the present computation has been depicted in Fig. 2.2. The index can be defined by the following formulations:

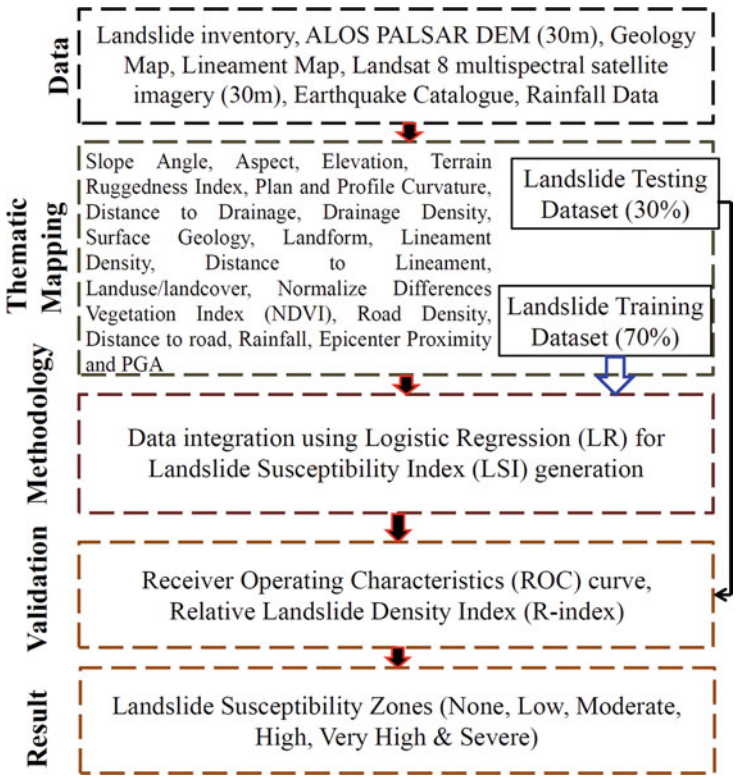

Fig. 2.2 Road Map of the algorithm worked out in the LR protocol employed here

$$Z = \beta_0 + \beta_1 X_1 + \beta_2 X_2 + \cdots + \beta_n X_n \tag{2.1}$$

Here Z denotes the linear logistic regression model. β_0 is a constant. β_1, β_2 are the corresponding coefficients of each of the respective contributing factors that indicate their contribution to landslide susceptibility. X_1, X_2 ,... X_n are the independent variables.

The probability index is calculated to predict the landslide hazard zone index; the possibility of occurrence and its intensity as

$$P = 1/(1 + \ell^{-z}) \tag{2.2}$$

Here P is the probability of landslide hazard index and Z takes any value from $-\infty$ to $+\infty$.

Accuracy Assessment

Receiver Operating Characteristic (ROC) is widely used for assessing the performance of the classification algorithms, employed in the extreme event computations. In geoscience, ROC is defined as a plot of test sensitivity or True Positive Rate (TPR) as the y-coordinate versus its 1-specificity or False Positive Rate (FPR) as x-coordinate at various threshold settings, which is a very effective method for evaluating the performance of dichotomy problems (Park et al., 2004; Fawcett, 2006). It is widely used in the validation of landslide susceptibility maps and also for estimating its accuracy. The area under ROC curve known as AUC is a common metric that can be used to compare different tests and the values, ranging from 0.5 to 1 which is widely employed to estimate the accuracy of the presence or absence of predictive models (Shahabi et al., 2014). An AUC close to 0.5 corresponds to a poor diagnostic test, and the larger the AUC, the more accurate is the test. The relative landslide density index (R-index) defined by Baeza and Corominas (2001) has been used to validate the susceptibility mapping results. R-index is defined as the ratio between the density of mass movements of a given susceptibility class and the overall mass movement density.

2.3 Results and Discussion

Thematic Layers Preparation

Landslide Inventory

Landslide inventory map of the terrain is prepared through multispectral satellite image interpretation, Google Earth imageries, published literature and reports from various government agencies, viz. Geological Survey of India (GSI); Nagaland State Disaster Management Authority; Disaster Management and Rehabilitation Department, Manipur; Remote Sensing Application Centre; and Bhuvan Portal developed by Indian Space Research Organization (n.d.). In the present study, multi-temporal satellite data and Google Earth imageries have been extensively used for the demarcation of a landslide accessible or inaccessible region in the hilly terrain. An extensive field survey has also been conducted to enlarge the inventory database as well as to validate the existing landslide inventory database. Through standard image analysis and field survey, a total of 4206 landslides have been identified. The landslide inventory database is randomly divided into subsets of 70% for training and 30% for testing as depicted in Fig. 2.1(c).

Morphometric Causative Factors

The topography is an essential factor for landslide susceptibility mapping that limits the density and spatial extent of landslides. The crucial morphological factors for the substantial causes of landslides are slope angle, elevation, aspect, plan and profile curvature, distance to drainage, drainage density and terrain ruggedness index (TRI). Slope failure is a very significant issue for landslide occurrence and is associated with slope movement due to gravitational forces (Catani et al., 2005). A slope angle is defined as an angle between the surface of the earth and a horizontal datum (Huang et al., 2017). At local scales, it affects the concentration of moisture and the level of pore pressure and is often used to resolve detailed patterns of instability. At larger scales, it controls regional hydraulic continuity and is considered an essential factor for GIS-based landslide susceptibility mapping (Guzzetti et al., 1999; Dai & Lee, 2002; Ohlmacher & Davis, 2003). The monotony of landslide occurrences can be defined by a morphometric slope based on the Topographic Gradient which is generated from the ALOS PALSAR digital elevation model (DEM). It is observed from the landslide inventory and slope angle database that the steeper the slope, the probability of mass failure increases in the region. In the present study, the slope angle varies from 0° to 76.6342°, as depicted in Fig. 2.3(a).

Elevation is another morphometric causative factor for landslide susceptibility mapping as several geological and geomorphological processes control it (Pourghasemi et al., 2012; Pradhan & Kim, 2014; Youssef et al., 2015). Landslides usually occur at intermediate elevation since slopes tend to be covered by a layer of thin colluvium that is prone to landslides (Dai & Lee, 2002). The altitude in the region is seen to vary from 26 to 3743 m, as shown in Fig. 2.3(b).

On the other hand, aspect is also pondered to have an augmented role in the mass movement, and it identifies the steepest downslope across a surface. The constraints associated with the Slope Aspect, such as the degree of saturation, discontinuities, drying winds and exposure to sunlight, may regulate the manifestation of a landslide. The slope aspect map is also obtained from ALOS PALSAR DEM and classified into nine standard directions, viz. flat, north, northeast, east, southeast, south, southwest, west and northwest, respectively, as depicted in Fig. 2.3(c).

The plan and profile curvature is defined as the rate of change of slope gradient or aspect, usually in a particular direction (Dikau, 1988; Wilson & Gallant, 2000; Nefeslioglu et al., 2008). The curvature value is evaluated by calculating the reciprocal value of the radius of curvature. Curvature is described as a contour formed by intersecting a horizontal plane with the surface. The impact of curvature on the slope erosion process is the convergence or divergence of water during downhill flow. Curvature has been used for landslide susceptibility mapping by Ayalew et al. (2004); Dikau (1988); Wilson and Gallant (2000); Nefeslioglu et al. (2008); Chen et al. (2017) and Ding et al. (2017). This parameter constitutes one of the causative factors in the present investigation as a vital factor, controlling landslide occurrences. The plan and profile curvatures have been prepared by using high-resolution DEM data, as depicted in Fig. 2.3(d and e).

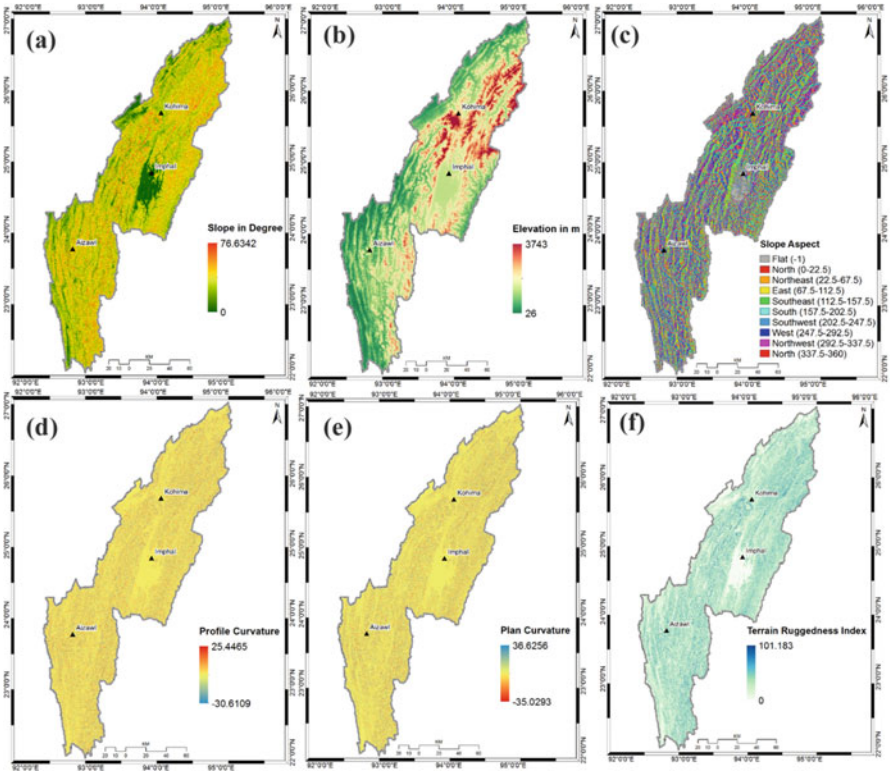

Fig. 2.3 GIS raster maps exhibit the morphometric causative factors of the terrain, viz. (**a**) Slope angle, (**b**) Elevation, (**c**) Slope Aspect, (**d**) Profile Curvature, (**e**) Plan Curvature and (**f**) Terrain Ruggedness Index (TRI)

The terrain ruggedness index is defined by the altitude variation between the adjacent cells of a digital elevation model (Alkhasawneh et al., 2013). The process determines the difference in altitude values between a centre cell and the surrounding cells. Then it squares each of the eight elevation difference values to make them all positive and then averages the squares. The terrain ruggedness index is then derived by taking the square root of this average, as shown in Fig. 2.3(f).

Drainage network is another causative factor for landslide occurrence and has been renowned as a topographic characteristic of fundamental importance. As the density of stream linkage reveals the geological, topographical, soil and the vegetation control, drainage network is chosen to simultaneously contemplate the undercutting of a hydrographic system for the role of inappropriate drainage (Shahabi et al., 2014). The proximity of the steep slope to the drainage network is an additional essential element controlling the slope stability because the streams adversely erode the material of the lower portion and make the proliferation of water level (Shahabi et al., 2014). The total length of the stream in a given section throughout its area provides drainage density, which has been calculated from the

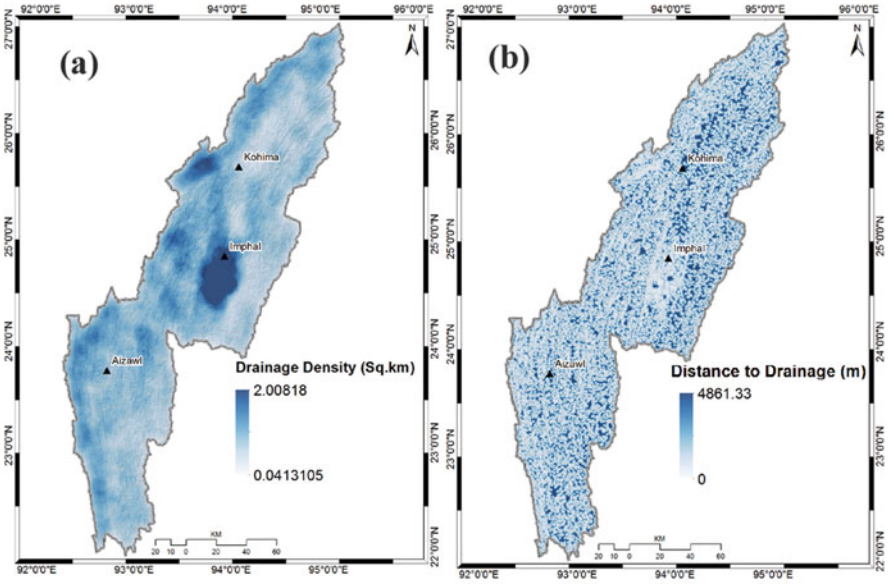

Fig. 2.4 GIS maps exhibit the morphometric causative factors of the terrain, viz. (**a**) Drainage Density and (**b**) Distance to Drainage

drainage network and is seen to vary from 0.0413105 to 2.00818 km^2 as depicted in Fig. 2.4(a). The drainage proximity varies between 0 and 4861.33 m as depicted in Fig. 2.4(b).

Geological Causative Factors

The surface geological attribution is considered as an independent variable in the present study. Various geological formations have different compositions and structures, which contribute to the strength and permeability of rocks and soils. The stronger rocks give more resistance to the driving forces as compared to the weaker rocks and hence are less prone to landslides. The major geological formation of the terrain belongs to Belt of Schuppen designated as (1) accretionary prism; (2) ophiolite/melange, (3) accetionary complex; (4) alluvial fill along foredeep; (5) alluvial fill along superposed basin; (6) crystalline complex overprinted by Himalayan fold-thrust movement; (7) and cover rocks of frontal belt affected by fold-thrust movement during the terminal phase of Himalayan geology (8) as shown in Fig. 2.5(a).

Landform defines the spatial topological interactions of landforms which involve segregating the terrain into intangible spatial objects such as chronology, composition and features. The numerous geomorphological features of the landscape have been derived from ALOS PALSAR DEM wherein various types of landforms, viz. plains, valleys, open slopes, upper slopes mesas, mountaintops high ridges, upland

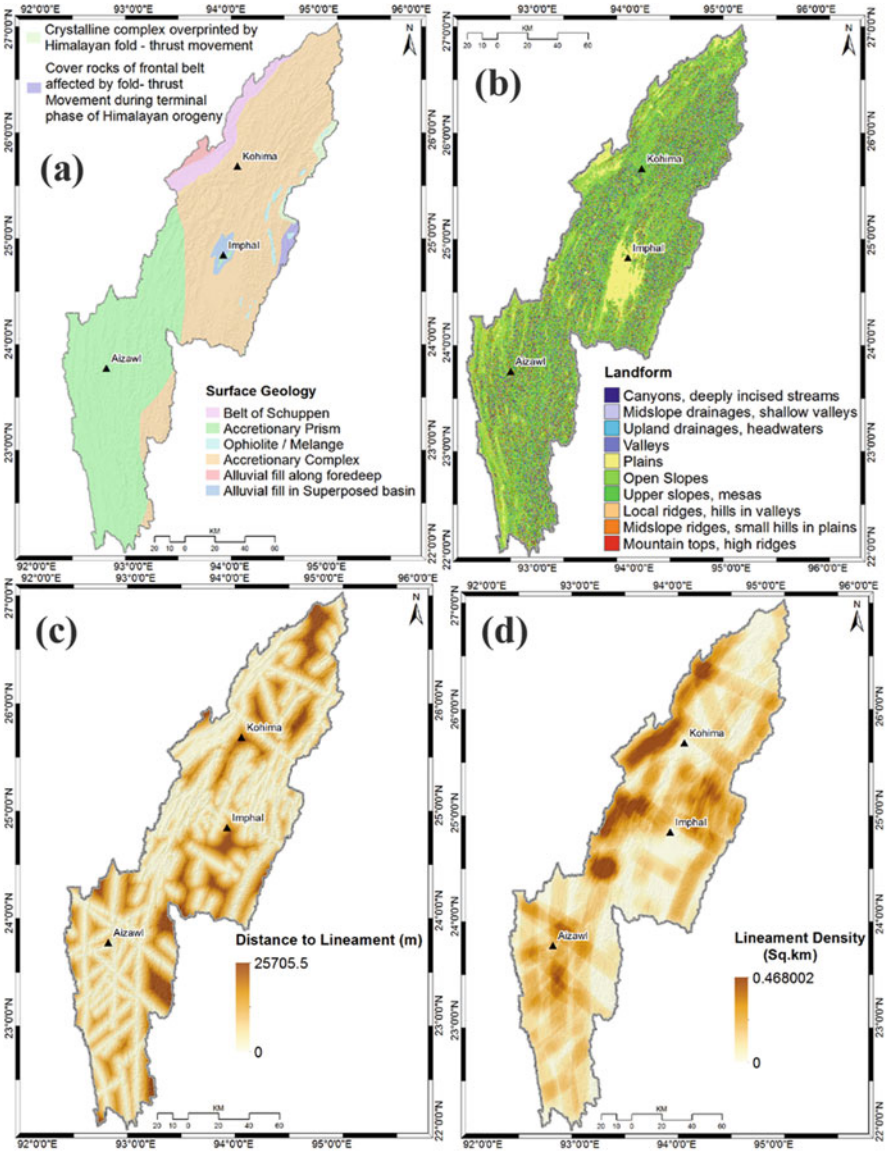

Fig. 2.5 GIS raster maps exhibit the geological causative factors of the terrain, viz. (**a**) Surface Geology, (**b**) Landform, (**c**) Distance to Lineament and (**d**) Lineament Density

drainages headwaters, midslope ridges small hills in plains, local ridges hills in valleys and canyons deeply incised streams and midslope drainages shallow valleys respectively following Jenness (2006) as depicted in Fig. 2.5(b).

The lineament is also an important contributing factor for the occurrence of a landslide as the degree of intense deformation, fracturing, fissures and weathering play crucial roles in causing slope failure (Bui et al., 2012). The disposition of structural discontinuities about slope inclination and direction has a great influence on the stability of slopes, which includes the extent of parallelism between the steepness and direction in the dip of discontinuity of the slope. Distance to lineament varies between 0 and 25,705.5 m, as shown in Fig. 2.5(c). The intensity of rock fracturing can be epitomized by lineament density, which is inevitable for the development of muffled passages over an area; therefore, the lineaments in the study region are mapped and analysed by lineament density and is seen to vary from 0 to 0.468 km^2 as depicted in Fig. 2.5(d).

Environmental Causative Factors

Normalized Differences Vegetation Index (NDVI) is an important causative factor for the movement of rainfall-induced landslides. Changes in vegetation cover often result in modified landslide behaviour (Van Beek, 2002; Wilkinson et al., 2002; Glade, 2003; Peduzzi, 2010). It is also a virtuous gage for the probability of mass movement. Vegetation roots penetrate the soil and increase their shear strength. The combination of recorded electromagnetic reflectance in near-infrared and red wavelength is highly correlated with the photosynthetic activity and the density of vegetation cover (Peduzzi, 2010). The NDVI map is prepared from Landsat 8 image through band ratio technique, i.e. near-infrared - Red/near-infrared + red, in which the index value ranges from −0.255 to 0.731. It is observed that the value of NDVI is comparatively higher in landslide-prone areas where there is a dense vegetation cover, such as the areas with heavy rainfall and the soil with the wet condition (Vakhshoori & Zare, 2016; Sonawane & Bhagat, 2017) as depicted in Fig. 2.6(a).

Landuse/landcover (LULC) plays a crucial role in the stability of the topographic gradient. Forest controls continuous water flow and regular infiltration; on the other hand, cropland and agricultural land affect slope stability owing to saturation of covered soil (Devkota et al., 2013; Regmi et al., 2014). In the present study, LULC map has been modified from GlobCover (2009) land cover map and classified into eight major LULC classes such as irrigated croplands, rainfed croplands, croplands/vegetation, vegetation/croplands, closed to open broadleaved evergreen or semi-deciduous forest, closed broadleaved deciduous forest, open broadleaved deciduous forest, closed needleleaved evergreen forest, closed to open mixed broadleaved and needleleaved forest, mosaic forest-shrubland/grassland, mosaic grassland/forest-shrubland, closed to open shrubland, closed to open grassland, artificial areas and water bodies as depicted in Fig. 2.6(b).

The road segmentation is a significant spot of anthropogenic instability and numerous road construction activities such as quarrying of soil, striking of additional load, vertical segmentation of slopes, dam construction and vegetation removal may lead to some tensional cracks due to an increase in stress on the back of the slope

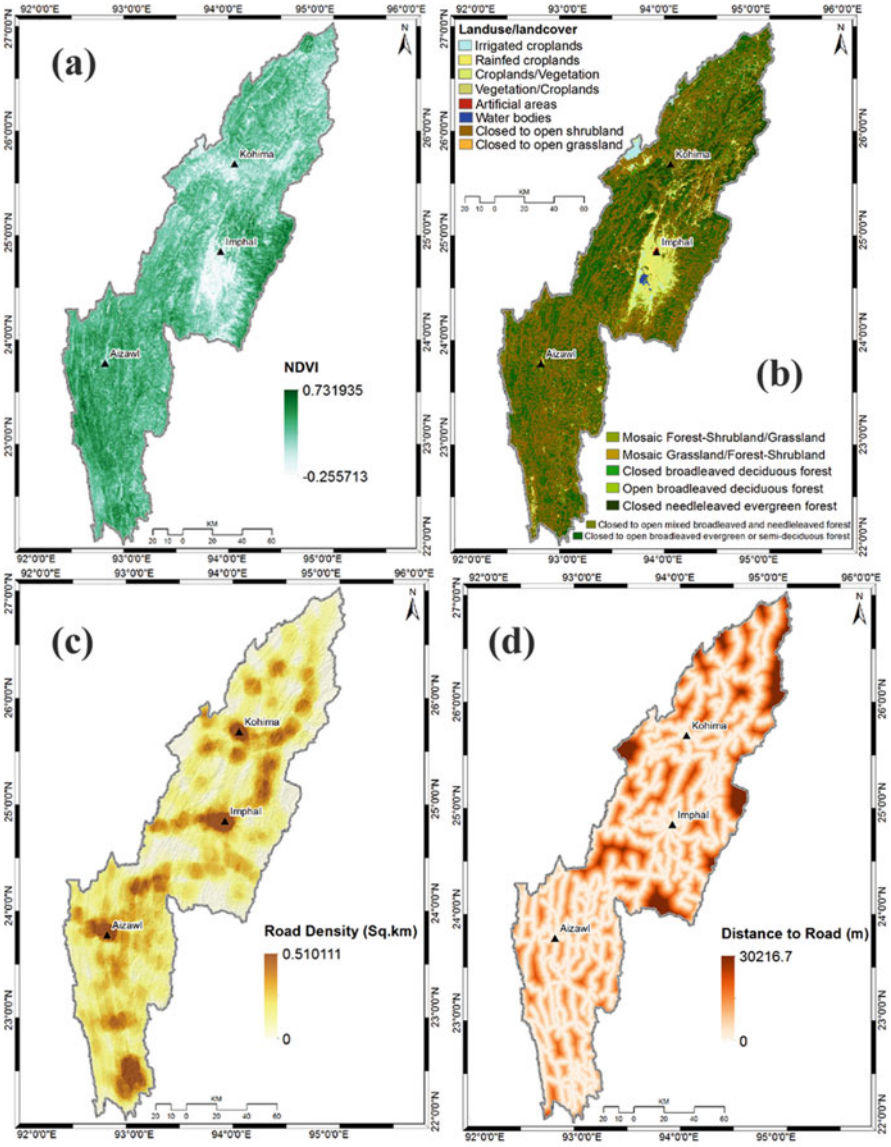

Fig. 2.6 GIS maps exhibit environmental causative factors of the terrain, viz. (**a**) Normalized Differences Vegetation Index (NDVI), (**b**) Landuse/landcover (LULC), (**c**) Road Density and (**d**) Distance to Road

which frequently serves as a cradle for the occurrence of landslides (Saadatkhah et al., 2014). In order to determine the effect of the road on the stability of slopes, various buffer zones are created on the path of the road from which the road density varies from 0 to 0.510 km^2 as shown in Fig. 2.6(c) and distance to road map has been

prepared on GIS platform and classified between 0 to 30216.7 m as depicted in Fig. 2.6(d). It is also observed that there is a significant correlation between the extent of landslides and the distance to the regional road system.

Triggering Causative Factors

In the Eastern Boundary Block of Northeast India, both the earthquake and rainfall are the major triggering factors responsible for landslide. The entire terrain falls under the active Himalayan seismogenic zone. The terrain has been affected by more than 800 μ to large-magnitude earthquakes (Nath et al., 2017). It is observed that the epicentre proximity plays a major role in the occurrence of a co-seismic landslide in this region. An epicenter proximity map has been generated using the Euclidean distance tool in the GIS platform, as shown in Fig. 2.7(a) that exhibits a variation from 0 to 34,096.1 m.

Surface consistent peak ground acceleration (PGA) is another important factor responsible for triggering co-seismic landslides in the region. The intensity of ground-shaking calculated from the maximum acceleration representing the seismic hazard level in the region is a severe factor in the co-seismic landslide. The PGA with a 10% probability of exceedance in 50 years with a return period of 475 years has been adopted from Nath and Thingbaijam (2012), which shows a variation of PGA 0.558–0.944 g as depicted in Fig. 2.7(b). In general, there is greater vibration near the epicentre, where many of the co-seismic landslides generally occur.

Rainfall is another triggering factor for the occurrence of a landslide because it controls the water content in the soil. The amount of precipitation and the number of landslides is directly proportional to the altitude of the terrain (Sabatakakis et al., 2013). The average annual rainfall distribution map has been prepared using inverse distance weighted (IDW) interpolation technique by considering the rainfall data of

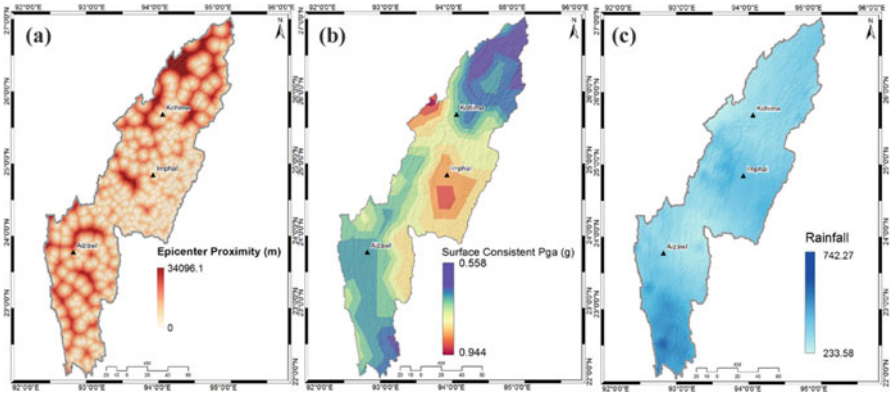

Fig. 2.7 GIS raster maps exhibit the triggering causative factors of the terrain: (**a**) Epicentre Proximity, (**b**) Surface Consistent Peak Ground Acceleration (PGA) with 10% probability of exceedance in 50 years with a return period of 475 years and (**c**) Average Annual Rainfall

the last 60 years (1950–2010), with a variation up to 233.58–742.27 mm/year as shown in Fig. 2.7(c). As per the data, it is observed that in the southern part of the region, the intensity of rainfall is high, while in the northern part, there is a low intensity of the precipitation.

Landslide Susceptibility Zonation Mapping by Using Multivariate Regression

In the present study, processing of data and factors has been carried out on the GIS Platform, while the statistical analysis by Logistic Regression has been performed using the Statistical Package for Social Sciences (SPSS). In the first step, 19 causative factors have been used for the independent variables dataset. All the causative factors have been exported to comma-separated values (CSV) format and imported into the statistical platform to achieve the regression coefficients, as shown in Table 2.2. The landslide inventory training dataset which is represented as a

Table 2.2 Causative factors and their coefficients derived through multivariate statistics-based logistic regression

Causative factors	β	S.E.	Wald	df	Sig.	Exp (β)
Landuse/landcover (LULC)	0.211	0.228	0.853	1	0.356	1.234
Surface geology	4.420	0.443	99.708	1	0.000	83.076
Rainfall (mm/year)	−0.004	0.000	105.028	1	0.000	0.996
PGA (g)	−6.029	0.518	135.398	1	0.000	0.002
Slope angle (degree)	0.052	0.007	58.140	1	0.000	1.053
Distance to drainage (m)	0.000	0.000	5.530	1	0.019	1.000
Terrain ruggedness index (TRI)	−0.006	0.012	0.246	1	0.620	0.994
Road density (km^2)	1.445	0.460	9.864	1	0.002	4.240
Profile curvature	0.029	0.031	0.872	1	0.350	1.029
Plan curvature	−0.031	0.031	0.943	1	0.332	0.970
Normalized difference vegetation Index (NDVI)	−3.007	0.432	48.456	1	0.000	0.049
Lineament density (km^2)	1.601	0.623	6.602	1	0.010	4.959
Elevation (m)	0.000	0.000	6.070	1	0.014	1.000
Epicentre proximity (m)	0.000	0.000	2.464	1	0.117	1.000
Distance to road (m)	0.000	0.000	137.183	1	0.000	1.000
Distance to lineament (m)	0.000	0.000	3.238	1	0.072	1.000
Drainage density (km^2)	−0.902	0.326	7.644	1	0.006	0.406
Aspect	−0.001	0.000	8.321	1	0.004	0.999
Landform	−0.005	0.115	0.002	1	0.964	0.995
Constant	2.309	0.650	12.613	1	0.000	10.061

S.E. standard error, *Wald* Wald chi-square values, *df* degree of freedom, *Sig*. significance, *Exp(β)* exponentiated coefficient

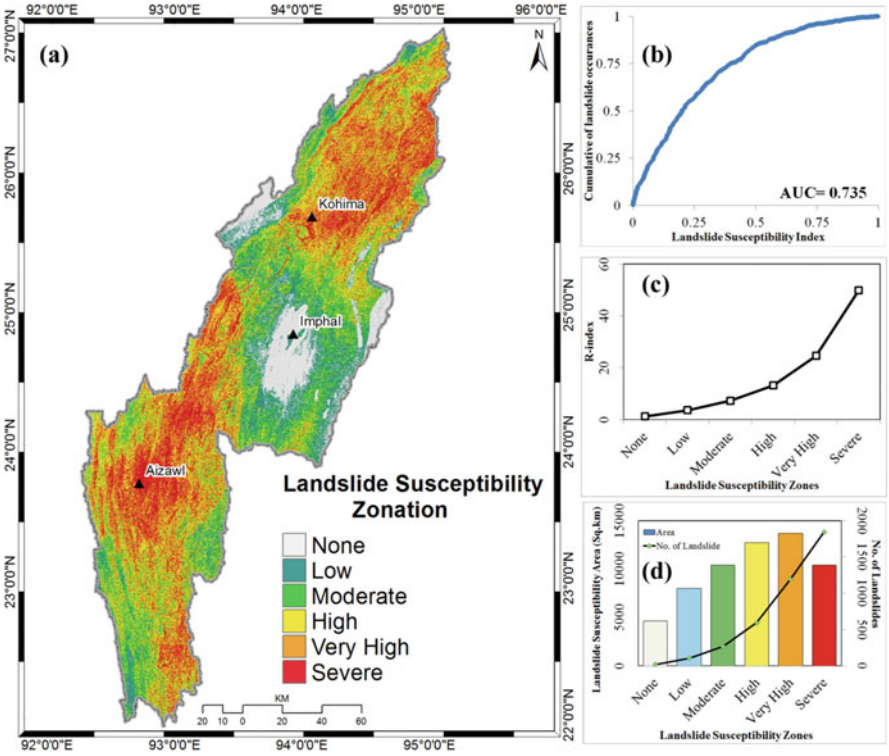

Fig. 2.8 (**a**) Landslide susceptibility map of the Eastern Boundary Block comprising of the States of Nagaland, Manipur and Mizoram of Northeast India classified into six susceptible zones; (**b**) ROC curve for the susceptibility map; graphs show the cumulative landslide occurrences versus landslide susceptibility index with AUC = 0.735, (**c**) relative landslide density index (R-index) of the LR-derived landslide map and (**d**) graph exhibiting the number of landslides (line graph) and landslide susceptibility zones area (bar graph)

dependent variable has been extracted after rasterizing polygons and then coding the cells falling in the landslide areas. In the LR analysis, cells could get attributes providing information on the presence or absence of the landslide phenomena within 30 × 30 m pixels. After integrating the coefficients, using both Eqs. (2.1) and (2.2), the proneness to landslide has been spatially distributed in the region. The logistic regression method is used to develop a landslide susceptibility zonation map for indicating locations where the probabilities of landslide occurrence varies from 0.0 to 1.0. Numbers closer to 1 indicate the probability of landslide occurrences. The susceptibility index map has been classified as none susceptible covering around 4622 km^2, low susceptibility covering around 8000 km^2, moderate susceptibility covering around 10,422 km^2, high susceptibility covering around 12,708 km^2, very high susceptibility covering around 13,702 km^2 and severe susceptibility covering around 10,415 km^2 as shown in Fig. 2.8(a). The urban, semi-urban centres and other

lifeline facilities, including major transportation facilities like national highways, state highways, have been severely affected due to frequent landslide in the terrain.

The accuracy statistics of logistic regression-based landslide susceptibility map in the terrain has been evaluated by receiver operating characteristics (ROC) and relative landslide density index (r-index) in the area versus the number of landslides plot as shown in Fig. 2.8(c and d). The accuracy of the model is developed in the area under the roc curve (AUC) values vary from 0.5 to 1.0 in the ROC statistics. Its ability to reliability predicts the occurrence and non-occurrence of an event, which is defined by the probabilistic model of AUC to apply the ROC statistics in the study region for testing landslide inventory dataset which has been prepared to use randomly selected landslide events from landslide and non-landslide locations. The AUC value of the ROC curve for LR is estimated to be 0.735, as depicted in Fig. 2.8(b).

2.4 Conclusion

Landslide susceptibility mapping is considered the most important step onward in landslide hazard mitigation and management in the terrain. Logistic regression method has been used to describe the spatial distribution of landslide susceptibility zonation on a medium scale of 1:50,000 with a spatial resolution of 30 m $\times$ 30 m. The accuracy assessment of multivariate statistics-based Logistic Regression (LR) technique is established by using receiver operating characteristics, relative landslide density index and landslide area versus number of landslide graph and by matching the susceptibility map with testing inventory dataset. Logistic regression method indicates that land use/land cover, surface geology, slope angle, road density and lineament density establish the most important conditioning factors in causing mass movement in the terrain. The susceptibility zonation map provides information that led to a major improvement in the understanding of the causes for densely scattering of landslides in the terrain. The landslide susceptibility zonation map prepare in the present study can help as a reference for city planners, architects and geotechnical engineers in land use planning and slope management.

References

Alkhasawneh, M. S., Ngah, U. K., Tay, L. T., Isa, M., Ashidi, N., & Al-batah, M. S. (2013). Determination of important topographic factors for landslide mapping analysis using MLP network. *The Scientific World Journal, 2013*, 1–13. https://doi.org/10.1155/2013/415023

Ayalew, L., Yamagishi, H., & Ugawa, N. (2004). Landslide susceptibility mapping using GIS-based weighted linear combination, the case in Tsugawa area of Agano River, Niigata Prefecture, Japan. *Landslides, 1*(1), 73–81. https://doi.org/10.1007/s10346-003-0006-9

Baeza, C., & Corominas, J. (2001). Assessment of shallow landslide susceptibility by means of multivariate statistical techniques. *Earth Surface Processes and Landforms: The Journal of the British Geomorphological Research Group, 26*(12), 1251–1263. https://doi.org/10.1002/esp.263

Bai, S., Lü, G., Wang, J., Zhou, P., & Ding, L. (2011). GIS-based rare events logistic regression for landslide-susceptibility mapping of Lianyungang, China. *Environmental Earth Sciences, 62*(1), 139–149.

Balamurugan, G., Ramesh, V., & Touthang, M. (2016). Landslide susceptibility zonation mapping using frequency ratio and fuzzy gamma operator models in part of NH-39, Manipur, India. *Natural Hazards, 84*(1), 465–488.

Barman, B. K., & Srinivasa Rao, K. (2019). Landslide hazard susceptibility mapping of upper Tuirial watershed, Mizoram using Remote Sensing and GIS techniques. *International Journal of Research and Analytical Reviews, 6*(1), 1624–1630.

Bhuvan Portal developed by Indian Space Research Organization. https://bhuvan-app1.nrsc.gov.in/disaster/disaster.php?id=landslide_monitor

Bui, D. T., Pradhan, B., Lofman, O., Revhaug, I., & Dick, O. B. (2012). Spatial prediction of landslide hazards in HoaBinh province (Vietnam): A comparative assessment of the efficacy of evidential belief functions and fuzzy logic models. *Catena, 96*, 28–40. https://doi.org/10.1016/j.catena.2012.04.001

Catani, F., Casagli, N., Ermini, L., Righini, G., & Menduni, G. (2005). Landslide hazard and risk mapping at catchment scale in the Arno River basin. *Landslides, 2*(4), 329–342. https://doi.org/10.1007/s10346-005-0021-0

Chen, W., Xie, X., Wang, J., Pradhan, B., Hong, H., Bui, D. T., & Ma, J. (2017). A comparative study of logistic model tree, random forest, and classification and regression tree models for spatial prediction of landslide susceptibility. *Catena, 151*, 147–160. https://doi.org/10.1016/j.catena.2016.11.032

CRED; EMDAT: http://www.emdat.be

Dai, F. C., & Lee, C. F. (2002). Landslide characteristics and slope instability modeling using GIS, Lantau Island, Hong Kong. *Geomorphology, 42*(3–4), 213–228. https://doi.org/10.1016/S0169-555X(01)00087-3

Dasgupta, S., Sural, B., Harendranath, L., Mazumadar, K., Sanyal, S., Roy, A., Das, L. K., Misra, P. S., & Gupta, H. (2000). *Seismotectonic atlas of India and its environs*. Geological Survey of India, Calcutta, India.

Devkota, K. C., Regmi, A. D., Pourghasemi, H. R., Yoshida, K., Pradhan, B., Ryu, I. C., & Althuwaynee, O. F. (2013). Landslide susceptibility mapping using certainty factor, index of entropy and logistic regression models in GIS and their comparison at Mugling–Narayanghat road section in Nepal Himalaya. *Natural Hazards, 65*(1), 135–165. https://doi.org/10.1007/s11069-012-0347-6

Dikau, R. (1988). Case studies in the development of derived geomorphic maps. *Geologisches Jahrbuch A, 104*, 329–338.

Dilley, M., Chen, R. S., Deichmann, U., Lerner-Lam, A. L., & Arnold, M. et al. (2005). *Natural disaster hotspots – a global risk analysis*. Report of the International Bank for Reconstruction and Development/The World Bank and Columbia University: 132.

Ding, Q., Chen, W., & Hong, H. (2017). Application of frequency ratio, weights of evidence and evidential belief function models in landslide susceptibility mapping. *Geocarto International*, *32*(6), 619–639.

Fawcett, T. (2006). An introduction to ROC analysis. *Pattern Recognition Letters, 27*(8), 861–874.

Froude, M. J., & Petley, D. N. (2018). Global fatal landslide occurrence from 2004 to 2016. *Natural Hazards and Earth System Sciences, 18*(8), 2161–2181.

Glade, T. (2003). Landslide occurrence as a response to land use change: A review of evidence from New Zealand. *Catena, 51*(3–4), 297–314. https://doi.org/10.1016/S0341-8162(02)00170-4

GlobCover. (2009). *Global land cover map*. http://due.esrin.esa.int/page_globcover.php

Guzzetti, F., Carrara, A., Cardinali, M., & Reichenbach, P. (1999). Landslide hazard evaluation: A review of current techniques and their application in a multi-scale study, Central Italy. *Geomorphology, 31*(1), 181–216. https://doi.org/10.1016/S0169-555X(99)00078-1

Guzzetti, F., Reichenbach, P., Ardizzone, F., Cardinali, M., & Galli, M. (2006). Estimating the quality of landslide susceptibility models. *Geomorphology, 81*(1–2), 166–184.

Hadmoko, D. S., Lavigne, F., & Samodra, G. (2017). Application of a semiquantitative and GIS-based statistical model to landslide susceptibility zonation in Kayangan Catchment, Java, Indonesia. *Natural Hazards, 87*(1), 437–468.

Huang, M. H., Fielding, E. J., Liang, C., Milillo, P., Bekaert, D., Dreger, D., & Salzer, J. (2017). Coseismic deformation and triggered landslides of the 2016 Mw 6.2 Amatrice earthquake in Italy. *Geophysical Research Letters, 44*(3), 1266–1274. https://doi.org/10.1002/2016GL071687

Jenness, J. (2006). Topographic Position Index (tpi_jen.avx) extension for ArcView 3.x, v. 1.3 a. Jenness Enterprises.

Khatsu, P., & Van Westen, C. J. (2005, November). Urban multi-hazard risk analysis using GIS and remote sensing: A case study from Kohima Town, Nagaland, India. In *Proceedings of the 26th Asian Conference on Remote Sensing*, pp. 7–11.

Laldintluanga, E. H., Lalbiakmawia, F., & Lalbiaknungi, E. R. (2016). International Journal of Engineering Sciences& Research Technology Landslide Hazard Zonation along State Highway between Aizawl City and Aibawk Town, Mizoram, India using Geospatial Techniques.

Lallianthanga, R. K., & Lalbiakmawia, F. (2013a). Landslide Hazard zonation of Aizawl district, Mizoram, India using remote sensing and GIS techniques. *International Journal of Remote Sensing & Geoscience, 2*(4), 14–22.

Lallianthanga, R. K., & Lalbiakmawia, F. (2013b). Micro-level landslide hazard zonation of Saitual Town, Mizoram, India Using Remote Sensing and GIS Techniques. *International Journal of Engineering Sciences & Research Technology, 2*(9), 2531–2546.

Lallianthanga, R. K., & Lalbiakmawia, F. (2014). Landslide susceptibility zonation of Kolasib District, Mizoram, India using remote sensing and GIS techniques. *International Journal of Engineering Sciences & Research Technology, 3*(3), 1402–1410.

Lallianthanga, R. K., & Laltanpuia, Z. D. (2014). Landslide hazard zonation mapping of Hnahthial Town, Mizoram, India. *Using Remote Sensing & GIS*.

Lallianthanga, R. K., Lalbiakmawia, F., & Lalramchuana, F. (2013). Landslide hazard zonation of Mamit town, Mizoram, India using remote sensing and GIS techniques. *International Journal of Geology, Earth & Environmental Sciences, 3*(1), 184–194.

Lee, S., & Pradhan, B. (2007). Landslide hazard mapping at Selangor, Malaysia using frequency ratio and logistic regression models. *Landslides, 4*(1), 33–41.

Mancini, F., Ceppi, C., & Ritrovato, G. (2010).GIS and statistical analysis for landslide susceptibility mapping in the Daunia area (Italy).

Mathew, J., Jha, V. K., & Rawat, G. S. (2009). Landslide susceptibility zonation mapping and its validation in part of Garhwal Lesser Himalaya, India, using binary logistic regression analysis and receiver operating characteristic curve method. *Landslides, 6*(1), 17–26.

Nandi, A., & Shakoor, A. (2010). A GIS-based landslide susceptibility evaluation using bivariate and multivariate statistical analyses. *Engineering Geology, 110*(1–2), 11–20.

Nath, S. K., & Thingbaijam, K. K. S. (2012). Probabilistic seismic hazard assessment of India. *Seismological Research Letters, 83*(1), 135–149.

Nath, S. K., Mandal, S., Adhikari, M. D., & Maiti, S. K. (2017). A unified earthquake catalogue for South Asia covering the period 1900–2014. *Natural Hazards, 85*(3), 1787–1810. https://doi.org/10.1007/s11069-016-2665-6

Nefeslioglu, H. A., Duman, T. Y., & Durmaz, S. (2008). Landslide susceptibility mapping for a part of tectonic Kelkit Valley (Eastern Black Sea region of Turkey). *Geomorphology, 94*(3–4), 401–418. https://doi.org/10.1016/j.geomorph.2006.10.036

Ohlmacher, G. C., & Davis, J. C. (2003). Using multiple logistic regression and GIS technology to predict landslide hazard in northeast Kansas, USA. *Engineering Geology, 69*(3–4), 331–343. https://doi.org/10.1016/S0013-7952(03)00069-3

Pachuau, L. (2019). Zonation of landslide susceptibility and risk assessment in Serchhip town, Mizoram. *Journal of the Indian Society of Remote Sensing, 47*(9), 1587–1597.

Park, S. H., Goo, J. M., & Jo, C. H. (2004). Receiver operating characteristic (ROC) curve: Practical review for radiologists. *Korean Journal of Radiology, 5*(1), 11–18. https://doi.org/10.3348/kjr.2004.5.1.11

Pathak, D. (2016). Knowledge based landslide susceptibility mapping in the Himalayas. *Geoenvironmental Disasters, 3*(1), 8.

Peduzzi, P. (2010). Landslides and vegetation cover in the 2005 North Pakistan earthquake: A GIS and statistical quantitative approach. *Natural Hazards and Earth System Sciences, 10*, 623–640. https://doi.org/10.5194/nhess-10-623-2010

Petley, D. (2012). Global patterns of loss of life from landslides. *Geology, 40*(10), 927–930.

Pourghasemi, H. R., Pradhan, B., & Gokceoglu, C. (2012). Application of fuzzy logic and analytical hierarchy process (AHP) to landslide susceptibility mapping at Haraz Watershed, Iran. *Natural Hazards, 63*(2), 965–996. https://doi.org/10.1007/s11069-012-0217-2

Pradhan, A. M. S., & Kim, Y. T. (2014). Relative effect method of landslide susceptibility zonation in weathered granite soil: A case study in Deokjeok-ri Creek, South Korea. *Natural Hazards, 72*(2), 1189–1217. https://doi.org/10.1007/s11069-014-1065-z

Regmi, A. D., Devkota, K. C., Yoshida, K., Pradhan, B., Pourghasemi, H. R., Kumamoto, T., & Akgun, A. (2014). Application of frequency ratio, statistical index, and weights-of-evidence models and their comparison in landslide susceptibility mapping in Central Nepal Himalaya. *Arabian Journal of Geosciences, 7*(2), 725–742. https://doi.org/10.1007/s12517-012-0807-z

Reichenbach, P., Rossi, M., Malamud, B. D., Mihir, M., & Guzzetti, F. (2018). A review of statistically-based landslide susceptibility models. *Earth-Science Reviews, 180*, 60–91.

Roy, J., Saha, S., Arabameri, A., Blaschke, T., & Bui, D. T. (2019). A novel ensemble approach for landslide susceptibility mapping (LSM) in Darjeeling and Kalimpong districts, West Bengal, India. *Remote Sensing, 11*(23), 2866.

Saadatkhah, N., Kassim, A., & Lee, L. M. (2014). Qualitative and quantitative landslide susceptibility assessments in Hulu Kelang area, Malaysia. *EJGE, 19*(47), 545–563.

Sabatakakis, N., Koukis, G., Vassiliades, E., & Lainas, S. (2013). Landslide susceptibility zonation in Greece. *Natural Hazards, 65*(1), 523–543. https://doi.org/10.1007/s11069-012-0381-4

Sema, H. V., Guru, B., & Veerappan, R. (2017). Fuzzy gamma operator model for preparing landslide susceptibility zonation mapping in parts of Kohima Town, Nagaland, India. *Modeling Earth Systems and Environment, 3*(2), 499–514.

Shahabi, H., Khezri, S., Ahmad, B. B., & Hashim, M. (2014). Landslide susceptibility mapping at central Zab Basin, Iran: A comparison between analytical hierarchy process, frequency ratio and logistic regression models. *Catena, 115*, 55–70. https://doi.org/10.1016/j.catena.2013.11.014

Singh, C. D., Behera, K. K., & Rocky, W. S. (2011). Landslide susceptibility along NH-39 between Karong and Mao, Senapati district, Manipur. *Journal of the Geological Society of India, 78*(6), 559–570.

Sonawane, K., & Bhagat, V. (2017). Improved change detection of forests using Landsat™ and ETM data. *Remote Sensing of Land 1*(1), 18–40. https://doi.org/10.21523/gcj1.17010102

Vakhshoori, V., & Zare, M. (2016). Landslide susceptibility mapping by comparing weight of evidence, fuzzy logic, and frequency ratio methods. *Geomatics Natural Hazards and Risk, 7*(5), 1731–1752. https://doi.org/10.1080/19475705.2016.1144655

Van Beek, L. P. H. (2002). *Assessment of the influence of changes in land use and climate on landslide activity in a Mediterranean environment*. Doctoral dissertation.

Wilkinson, P. L., Anderson, M. G., & Lloyd, D. M. (2002). An integrated hydrological model for rain-induced landslide prediction. *Earth Surface Processes and Landforms: The Journal of the British Geomorphological Research Group, 27*(12), 1285–1297. https://doi.org/10.1002/esp.409

Wilson, J. P., & Gallant, J. C. (2000). *Terrain analysis: Principles and applications*. Wiley.

Youssef, A. M., Pradhan, B., Jebur, M. N., & El-Harbi, H. M. (2015). Landslide susceptibility mapping using ensemble bivariate and multivariate statistical models in Fayfa area, Saudi Arabia. *Environmental Earth Sciences, 73*(7), 3745–3761.